Matter and Radiation at Extremes | RESEARCH ARTICLE | scitation.org/journal/mre

Application of quantum-statistical methods to studies of thermodynamic and radiative processes in hot dense plasmas

Cite as: Matter Radiat. Extremes 4, 054403 (2019); doi: 10.1063/1.5096439
Submitted: 18 March 2019 • Accepted: 19 June 2019 •
Published Online: 21 September 2019

Nikolay Yu. Orlov,[1] Maxim A. Kadatskiy,[1,2] Oleg B. Denisov,[1] and Konstantin V. Khishchenko[1,2]

AFFILIATIONS

[1]Joint Institute for High Temperatures of the Russian Academy of Sciences, Izhorskaya 13 Bldg 2, Moscow 125412, Russia
[2]Moscow Institute of Physics and Technology, Institutskiy Pereulok 9, Dolgoprudny, Moscow Region 141701, Russia

ABSTRACT

Calculations of thermodynamic and radiative characteristics of hot dense plasmas within different quantum-statistical approaches, such as the use of the Hartree–Fock–Slater model and the ion model, are presented. Calculated equations of state of different substances are used to investigate findings from absolute and relative measurements of the compressibility of solid aluminum samples in strong shock waves. It is shown that our calculated Hugoniot adiabat of aluminum is in a good agreement with experimental data and other theoretical results from first principles. We also present a review of the most important applications of the quantum-statistical approach to the study of radiative properties of hot dense plasmas. It includes the optimization problem of *hohlraum* wall materials for laser inertial fusion, calculations of the radiative efficiency of complex materials for optically thin plasma in X-pinch, modeling of radiative and gas-dynamic processes in plasma for experiments, where both intense laser and heavy ion beams are used, and temperature diagnostics for X- and Z-pinch plasmas.

I. INTRODUCTION

Active experimental and theoretical research on the thermodynamic and radiative properties of hot dense plasma has been carried out during recent years to reach a deeper understanding of the physical processes, which occur when matter goes into a high energy density state.[1–11] Such a state can be obtained by the use of explosive generators of intense shock waves,[12–14] magnetically accelerated flyers,[15,16] high power laser pulses interacting with targets or *hohlraum* walls in laser inertial fusion experiments,[17–21] as well as exploding wires at X- and Z-pinches,[22–27] and high-energy particle beams produced by an accelerator.[28–32] Before adoption of the Comprehensive Nuclear Test Ban Treaty by the United Nations General Assembly in 1996, a large set of experimental data produced using underground nuclear explosions had been collected.[33–37]

Basic theoretical study of these physical processes has to include important components, namely gas-dynamics, photon transport processes, the equation of state, and radiative opacity of hot dense matter.[38] It should be noted that the radiative opacity as well as equation of state represent especially important parts of this study.[39–42] Therefore, modern quantum mechanical methods have a strong influence on progress in these scientific directions.

To construct the equation of state of matter for a wide range of temperatures and densities, the Hartree–Fock–Slater (HFS) model[43] has been successfully used. In this paper, an equation of state calculated within the HFS model is applied to study the compressibility of condensed matter in strong shock waves. The experiments under consideration[37] correspond to states at high pressures and temperatures, where the approximations used in this model are valid.

An important and separate issue is to calculate the properties of mixtures of various chemical elements (compounds, alloys etc).[44] For radiative properties of such substances, the use of the average atom approximation of the HFS model is not enough. In particular, even small impurities can dramatically change the opacity factor of the material.[45]

It should be noted that intensive theoretical study in the field of many-body problems in quantum mechanics and the density-functional theory[46–49] have enabled the development of a modern quantum-statistical model, which is known as the ion model of plasma (IM).[50,51] Important features of this model are considered and discussed. The model was applied to calculate the radiative opacity characteristics of plasma in different studies, in the field of laser and heavy ion inertial fusion, to study radiative properties of plasma of

exploding wires at X- and Z-pinches, for temperature diagnosis of plasma. A review of the most important results is presented in this paper.

II. QUANTUM-STATISTICAL METHODS

Different quantum-statistical models and corresponding computer codes have been developed recently to calculate thermodynamic and radiative characteristics of plasmas, such as spectral coefficients for x-ray absorption, the Planck and Rosseland mean free paths for plasmas of pure elements and complex chemical compositions. Thus, the following models have been proposed and developed: the Thomas–Fermi (TF) model,[52–54] the Thomas–Fermi with corrections (TFC) model,[55,56] the Hartree–Fock–Slater model,[57,58] the detailed configuration accounting (DCA) model,[59] and its modern version, the detailed level-accounting (DLA) model.[60]

The TF model is the first and the simplest quantum-statistical model. Within the framework of this model, it is assumed that the electrons are continuously distributed in phase space according to the Fermi–Dirac distribution.[52,53] The TF model was first formulated for a cold free atom, and then generalized to arbitrary temperatures and densities by means of the approximation of the average atom.[54] For this approximation, instead of a set of ions with different electron configurations, a single ion with average occupation numbers is considered. Unfortunately, physical approximations, which provide a solution of the TF model equations, restrict the range of physical parameters, temperature and density, over which the model can be applied. The equations of the TF model correctly describe the behavior of matter in the limiting cases of strong compression, where the matter behaves as a degenerate Fermi gas, and at high temperature, where the electron gas is nearly uniform and ideal.[61]

The TF model can be improved by incorporation of the exchange and quantum corrections of second order in $\hbar$, which gives the equations of the TFC model.[55] The values of these corrections should be small in comparison with the original values of the TF model. The TFC model therefore has the same restrictions as the TF model.

In the HFS model, electrons with a discrete energy spectrum are recorded in a wave function form, whereas exchange energy and electrons with a continuous spectrum are taken into account by the semiclassical approximation. Under this approach, an atomic system with noninteger numbers of bound and band[62] electrons in the atomic shells is considered instead of real atomic or ionic systems. The HFS model application has a definite temperature restriction. If the temperature of the plasma decreases, this model cannot provide good enough results.[63] It should be noted that in the framework of the HFS approximation, one can consider the influence of individual states of ions by the application of the perturbation theory. However, this imposes temperature and density restrictions, which depend on the specific chemical element. This leads to difficulties in applying this model to complex chemical compositions of plasmas.

The DCA model[59] uses the Hartree–Fock equations to consider huge numbers of atomic and ionic electron configurations in a real plasma ensemble instead of only one average atom. The Saha method is used for calculating the concentrations of atoms and ions. This approach cannot be used for strongly coupled plasmas because of a specific character of the Saha method. The recent modification of this approach, the DLA model,[60] uses experimental data on quantum characteristics of ionic and atomic systems instead of solutions of the Hartree–Fock equations.

It is important to note that a high power laser pulse can produce intense shock waves and intense radiation waves in the laser target.[21,64] As a result, a strongly coupled plasma can be produced.[20,65,66] This can lead to considerable deviation of atom and ion concentrations from the Saha distribution, and, moreover, to deviation of atomic and ionic quantum characteristics from the characteristics that are calculated or measured for an ideal or weakly coupled plasma. This fact can considerably reduce the accuracy of predictions based on this type of plasma model.

One can conclude that physical approximations, which are used to provide the solutions of equations in the TF, TFC, HFS, DCA, and DLA models, considerably restrict the range of plasma parameters, temperature and density, over which these models can provide good enough results. These circumstances obstruct the application of these models to the solution of the radiative gas-dynamics equations, since numerical solution of these equations requires data on the plasma radiative properties in the entire range of temperatures and densities.

As was mentioned above, intensive theoretical study in the field of many-body problems in quantum mechanics and the density-functional theory[46–49] has allowed the development of a modern quantum-statistical model, which is known as the ion model,[50,51] and this model has not restricted ranges of plasma parameters (with the exception of the low-temperature range $T \lesssim 10$ eV), such as the mentioned above models have.

The general set of self-consistent field equations that describe the quantum states of the entire ensemble of plasma atoms and ions has been obtained based on the density-functional theory. This set contains the Hartree–Fock equations for all atoms and ions with different electron configurations, the Gibbs distribution for concentrations of plasma atoms and ions, and the electroneutrality condition.[49]

The important feature of this set is the general coupling of all equations for all plasma atoms and ions, including excited states. It would appear that the set cannot be solved because of the huge number of equations. Nevertheless, the problem has been solved for pure elements.[50] Subsequently, it was applied to complex chemical compositions.[51] As a result, reliable quantum-statistical calculations of radiative opacity became possible over a wide range of plasma temperatures and densities.

III. CALCULATIONS OF THERMODYNAMIC PROPERTIES OF HOT DENSE PLASMAS

The calculation of thermodynamic properties is less sensitive to the detailed accounting of individual states of ions than the calculation of radiative properties.[67] It is therefore preferable to apply the simpler average atom approximation (the TFC or HFS model) to construct the equation of state.

The quantum-statistical models provide only the electronic part of the thermodynamics of the matter, which includes the thermal motion of electrons as well as the electron–electron and the electron–ion interactions. As well as the electronic part, it is necessary to take into consideration the thermal motion of the ions and ion–ion interactions by using an additional model for the ionic subsystem.

The simplest approach, to take into account only the thermal motion of ions without ion–ion interaction, is to apply the Boltzmann

ideal gas (IG) model.[68] This model can be used to describe the behavior of matter at sufficiently high temperatures and low (gas) densities. For dense matter, however, the IG model is rather inaccurate. Therefore models that can take into account the interaction between ions are also required.

It is possible to take into account ion–ion interaction by considering ions as point charged particles in the framework of the one-component plasma (OCP) model.[69] Nevertheless, if the finite size of the ions is comparable with the interatomic distances (as is the case at sufficiently high densities), this approach is not applicable. To take into account the influence of the finite size of the ion core, one can use the charged hard spheres (CHS) model.[70] It is important to note that equations of the OCP and CHS models were derived under the approximation of identical particles, and are not applicable to the case of compounds.

In the present paper, calculations of Hugoniot adiabats were carried out. Investigation of the shock compressibility is a convenient way to study equations of state of different types of materials due to the fact that the conservation laws provide expressions of the thermodynamic properties in the form of a one-dimensional kinematic dependence $D = f(U)$, where U is the mass (particle) velocity and D is the shock velocity.[38] Moreover, there are experimental data available in the region of applicability of the quantum-statistical approach, where the temperature and density are sufficiently high.[37,71]

A. Absolute measurements of the shock compressibility of aluminum

Absolute methods of determining the shock compressibility are based on simultaneous and direct measurements of the shock wave velocity D and the velocity U of the matter behind the front. The mass, momentum, and energy conservation laws yield directly the density ρ, the pressure P, and the specific internal energy E of the matter on the Hugoniot adiabat:[38]

$$\rho = \frac{D}{D-U}\rho_0, \tag{1}$$

$$P = \rho_0 DU + P_0, \tag{2}$$

$$E = \frac{1}{2}(P+P_0)\left(\frac{1}{\rho_0}-\frac{1}{\rho}\right) + E_0, \tag{3}$$

where ρ_0, P_0 and E_0 are the correspondent parameters in the initial state before the shock wave front.

In the range of pressures up to 1 TPa, the shock compressibility can be determined quite reliably in an absolute or quasi-absolute way. We summarized experimental data[15,72–76] to derive the dependence

$$D_{\mathrm{Al}} = A_0 + A_1 U_{\mathrm{Al}} + A_2 U_{\mathrm{Al}}^2, \quad 0 \leqslant U_{\mathrm{Al}} \leqslant U^*, \tag{4}$$

$A_0 = 5.2828$ km/s, $A_1 = 1.442$, $A_2 = -0.021\,524$ s/km, which passes smoothly into the calculated HFS+CHS Hugoniot curve of aluminum[77] (Table I) at joining point $U^* = 6.6855$ km/s, i.e., at $P^* = 253.13$ GPa.

For pressures greater than 1 TPa, the shock compressibility can be determined by the (absolute) γ-marker method, based on the use of strong fluxes of radiation specific to nuclear explosions.[78–81] However, this method is associated with higher measurement errors than methods used at lower pressures.

Hugoniot adiabats of aluminum[77] ($\rho_0 = 2.712$ g/cm^3, $P_0 = 0.1$ MPa, $E_0 = -12.1$ kJ/g) over the whole range of parameters investigated, calculated with different methods taking into account electronic and ionic contributions to the equation of state, are presented in Fig. 1. Here, in the region of maximum achievable compression, we can observe the qualitatively different behavior of the TFC and HFS models. The oscillatory behavior of Hugoniots calculated with the HFS model is caused by the consequent ionization of electron shells at increasing temperature, whereas the TFC model does not take into account the shell structure of atoms. In the region of influence of these effects on the Hugoniot of aluminum, there is no reliable experimental data that would confirm these oscillations with sufficient accuracy ($\Delta D/D \lesssim 0.005$).[77] Nevertheless, first-principles simulations using a combination of the path-integral Monte-Carlo method and the density-functional-theory molecular dynamics approach[82] (PIMC+DFT-MD) yield oscillations of the same magnitude as the HFS+CHS model in contrast to other quantum-statistical models under consideration.

The calculated difference between shock and mass velocities in shock-compressed aluminum for the experimental range of parameters is shown in Fig. 1(b). Scattering of experimental data from absolute measurements does not allow one to choose the best model in the whole available range of parameters, but for mass velocities $5 < U_{\mathrm{Al}} < 10$ km/s the HFS model has better agreement with experimental data compared to the TFC model.

TABLE I. Compression ratio ρ/ρ_0 on principle Hugoniot of aluminum, as a function of pressure $P = 10^{n+d}$ GPa, calculated by the HFS+CHS model with $\rho_0 = 2.712$ g/cm^3, $P_0 = 0.1$ MPa, $E_0 = -12.1$ kJ/g.

d	$n = 2$	$n = 3$	$n = 4$	$n = 5$	$n = 6$
0.0	1.524	2.782	4.507	4.732	4.457
0.1	1.608	2.945	4.626	4.683	4.363
0.2	1.701	3.102	4.722	4.677	4.287
0.3	1.803	3.261	4.794	4.725	4.228
0.4	1.915	3.436	4.844	4.797	4.181
0.5	2.036	3.627	4.873	4.853	4.144
0.6	2.167	3.825	4.880	4.861	4.115
0.7	2.308	4.018	4.867	4.804	4.092
0.8	2.458	4.200	4.834	4.695	4.073
0.9	2.617	4.364	4.784	4.570	4.058

B. Relative measurements of the compressibility of aluminum in strong shock waves

The maximum pressures in shock compression experiments have been achieved by the impedance-match method.[37] In such experiments, a shock wave passes through the shield from standard material and then reaches the surface of the investigated sample. After that, the isentropic unloading wave (in the case where the dynamic impedance $\rho_0 D$ of the investigated material is smaller than that of the standard material) or the second shock wave (otherwise) reflects back to the standard material with the same pressure as is behind the shock wave front in the investigated material. The shock wave velocities in the standard material (D_{std}) and in the investigated sample (D_{smp}) are measured.[38]

In the present work, the analysis of the results of relative measurements of the compressibility of aluminum (as the

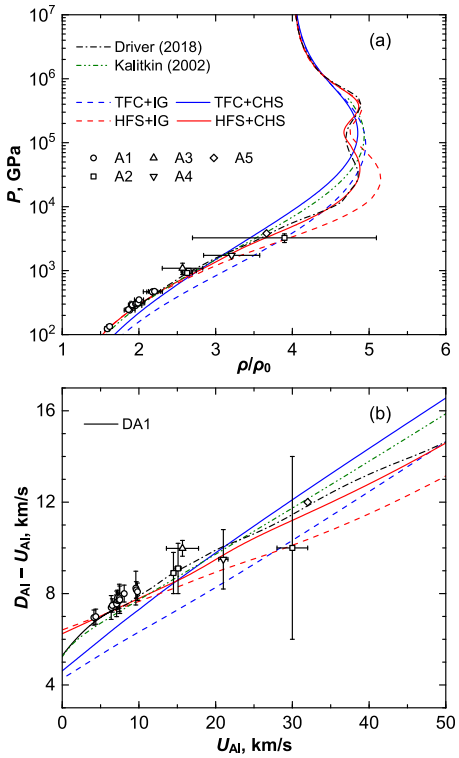

FIG. 1. The principal Hugoniot adiabatic curve of aluminum calculated using the TFC (blue) and HFS (red) models with different ionic contributions (IG—dashed lines; CHS—blue and red solid lines) in comparison with experimental data from absolute Hugoniot measurements (A1,[15] A2,[78] A3,[79] A4,[80] A5[81]) and results of other models, including the PIMC+DFT-MD model[82] (black dash-dot line), the semiempirical TFC-based approximation[71] (dark green dash-dot-dot line), and the semiempirical HFS+CHS-based approximation of experimental data[15,72–76] [Eq. (4), black solid line DA1] in coordinate planes (a) P vs ρ/ρ_0 and (b) $D - U$ vs U.

investigated material) in strong shock waves from nuclear[83–88] and chemical[89,90] explosions is carried out. Iron (Fe), molybdenum (Mo), and quartz (SiO_2) are chosen as standard materials.

Hugoniots of iron,[91] molybdenum,[108] and quartz[92] (with initial parameters listed in Table II), and corresponding unloading isentropes, were constructed within the four combinations of one of the two quantum-statistical models for electronic subsystems (TFC or HFS) and one of the two models for ionic subsystems (IG or CHS). The calculations of the compressibility of the sample and standard materials are performed relative to the range of shock velocities in aluminum from 10 to 500 km/s, which approximately corresponds to pressures in the investigated samples from 0.1 to 500 TPa. This range covers the maximum attainable values for pressures experimentally observed.[88]

Calculation results are also compared with previously proposed empirical dependences $D_{Al} = f(D_{std})$ having a form

$$D_{Al} = B_0 + B_1 D_{std} + B_2 D_{std}^2 + B_3 D_{std}^3 \quad (5)$$

within the range

$$D_1 \leqslant D_{Al} \leqslant D_2, \quad (6)$$

for the iron and quartz standards with coefficients from Refs. 37, 83, and 86 listed in Table II.

A detailed comparison of the calculated ratio D_{Fe}/D_{Al} with data from relative experiments on shock compression of aluminum in the range of parameters studied is illustrated in Fig. 2(a). By taking into account the scatter of experimental points,[86,87,89,90] it is possible to declare that the HFS+IG and HFS+CHS combinations of models provide the best agreement with experimental data at $15 \lesssim D_{Al} \lesssim 100$ km/s among the models considered, which indirectly confirms the existence of a significant influence of shell effects on thermodynamic properties of hot dense plasma.[87] Nevertheless, in the range of shock velocities $100 \lesssim D_{Al} \lesssim 1000$ km/s, where the predicted magnitude of oscillations is maximal, neither semiclassical (TFC) nor quantum mechanical (HFS) calculations contradict the available experimental data from Ref. 88.

Figure 2(b) shows the calculated ratio D_{Mo}/D_{Al}. Results from both the TFC and HFS models are in agreement with available experimental data[84,85] but, for lower shock velocities, these models do not agree with the experimental data from Ref. 93. To estimate the discrepancy, we construct the dependence in the form of Eq. (5) within the range

$$D_3 \leqslant D_{std} \leqslant D_4, \quad (7)$$

which is based on the approximation of data from absolute measurements of the shock compressibilities of aluminum and molybdenum, and obtain the coefficients listed in Table II. In this case, instead of building up unloading isentropes of molybdenum, it was assumed that, in the P–U coordinates, unloading isentropes are approximated with reasonable accuracy by specular reflection of the Hugoniot curves (the so-called reflection method).[94] For Hugoniot adiabats of molybdenum calculated using the TFC and HFS models, this assumption is justified at shock velocities $D_{Mo} \lesssim 20$ km/s.

When the dynamic impedance of an investigated sample is approximately equal to the dynamic impedance of a standard

TABLE II. Initial density and specific internal energy of standard materials at $P_0 = 0.1$ MPa used in our calculations as well as parameters from Refs. 37, 83, and 86 (iron, quartz) for Eqs. (5) and (6) and from this work (molybdenum) for Eqs. (5) and (7).

Standard	ρ_0 (g/cm^3)	E_0 (kJ/g)	B_0 (km/s)	B_1	B_2 (s/km)	B_3 (s^2/km^2)	D_1 (km/s)	D_2 (km/s)	D_3 (km/s)	D_4 (km/s)
Fe[86]	7.85	−7.452	0.614	1.1377	0.000 8	0	13.87	107.1	11.558	88.135
Quartz[83]	2.65	−9.74	3.761	0.735	0.004 16	0	12	32.55	10.576	33.004
Quartz[37]	2.65	−9.74	3.3	0.81	0	0	8	16	5.8	15.7
Quartz[37]	2.65	−9.74	0.9	0.96	0	0	16	34	15.7	34.5
Mo	10.22	−6.856	−2.0381	1.6098	−0.019 105	0.000 381 05	10.5672	26.7599	8.55	20.915

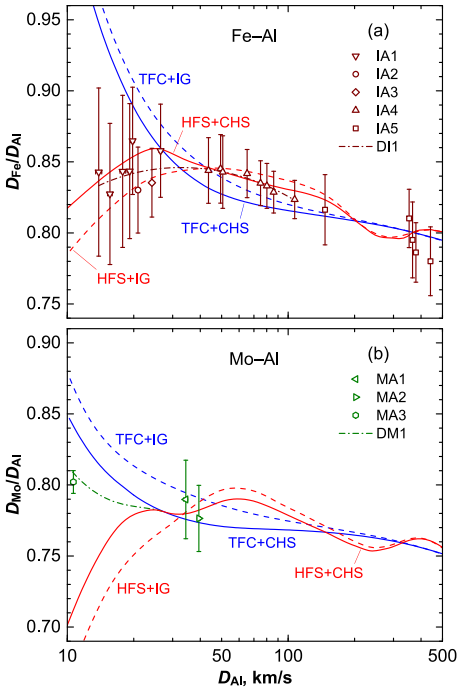

FIG. 2. Ratios D_{std}/D_{Al} as functions of D_{Al} for the impedance matching technique, where Al is the sample material and (a) Fe and (b) Mo are chosen as the standard materials. Calculated curves are obtained with the electronic part of the equations of state for the sample and the standards taken from the TFC (blue lines) and HFS (red lines) models and the ionic part from the IG (dashed) and the CHS (solid lines) models, as well as with empirical dependences $D_{Al}(D_{Fe})$[86] (dark red dash-dot line DI1[86]) and $D_{Al}(D_{Mo})$ (dark green dash-dot line DM1) in the form of Eq. (5) with coefficients from Table II. Experimental data correspond to standards of Fe (IA1,[86] IA2,[89] IA3,[90] IA4,[87] IA5[88]) and Mo (MA1,[84] MA2,[85] MA3[93]).

material, it is possible to use the reflection method over a broader range of parameters. In particular, it is justified in the case of relative experiments on compression of quartz and aluminum (Fig. 3). For this pair of materials, the distinction between calculated unloading isentropes and specular reflection of the corresponding Hugoniot adiabat of quartz is negligible over the whole investigated range of shock velocities.

It should be noted that it is a very convenient approach to use the D_{smp}–D_{std} coordinates as the direct representation of the primary experimental results.[33] This also yields an almost straight line over a wide range of wave velocities (Fig. 4). Observed deviation of the results from this line can serve as a criterion for the validity of experimental measurements.

To determine the mass velocity U and other shock wave parameters in the investigated material, knowledge of the equation of state of the standard material is required. In this paper, interpretations of experimental data[84–90] were revised by means of the HFS+CHS equations of state of iron and molybdenum. The values of shock wave parameters U_{Al}^{revis}, P_{Al}^{revis}, and ρ_{Al}^{revis}/ρ_0 obtained are listed in Tables III and IV and also compared with original[84,85,87–90] and other[95] interpretations of experiments ($U_{Al}^{of\ ref}$) and theoretical Hugoniots calculated using the HFS+CHS (U_{Al}^{theor}) and PIMC+DFT-MD models (Fig. 5).

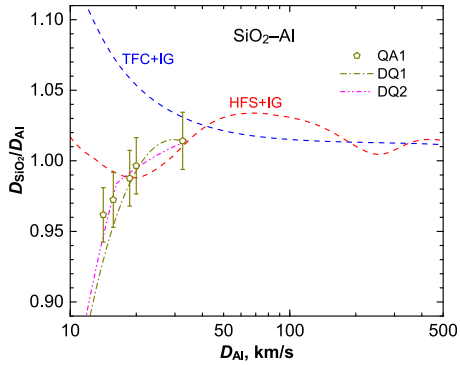

FIG. 3. Ratio D_{SiO_2}/D_{Al} as a function of D_{Al} for the impedance matching technique, where aluminum is the sample material and quartz is the standard material. Equations of state for aluminum and quartz are calculated using the TFC+IG (blue dashed line) and HFS+IG (red dashed line) models. Markers QA1 denote experimental data.[83] Empirical dependences $D_{Al}(D_{SiO_2})$ in the form of Eq. (5) with coefficients from Table II (dark yellow dash-dot line DQ1[83] and magenta dash-dot-dot line DQ2[37]) are shown as well.

IV. APPLICATIONS OF QUANTUM-STATISTICAL METHODS FOR CALCULATIONS OF THE RADIATIVE OPACITY OF HOT DENSE PLASMAS

A. Optimization of hohlraum wall materials for laser inertial fusion

As is known, the efficiency of *hohlraum* walls represents an important problem for laser inertial fusion since this factor rules the conversion energy of high power laser pulse into soft x-ray radiation. It has been shown[96] that *hohlraum* wall loss energy increases proportionally to the square root of the Rosseland mean free path:

$$\Delta E \propto \sqrt{l_R}. \tag{8}$$

The efficiency of *hohlraum* walls increases with a decrease of this value. Greater efficiency can be achieved by minimizing the Rosseland

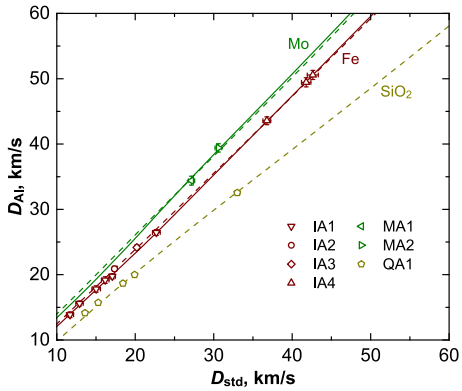

FIG. 4. Functions $D_{Al} = f(D_{std})$ for different standard materials: iron (dark red), molybdenum (dark green), and quartz (dark yellow). Calculations are based on the HFS electronic model with the CHS (solid lines) and IG (dashed lines) ionic part. Sources of experimental data are denoted in the captions to Figs. 2 and 3.

TABLE III. Measured shock velocities D in standard and sample materials for Fe–Al pair[86–90] with corresponding mass velocities U^{theor} calculated using the HFS+CHS model along with the results of previous interpretation[87–90,95] of $U_{Al}^{of\ ref}$ and our revision of U^{revis}, P^{revis} and ρ^{revis}/ρ_0 in shock-compressed samples calculated by means of construction of the release isentropes of the standard material using the HFS+CHS model.

D_{Fe} (km/s)	U_{Fe}^{theor} (km/s)	D_{Al} (km/s)	U_{Al}^{theor} (km/s)	$U_{Al}^{of\ ref}$ (km/s)	U_{Al}^{revis} (km/s)	P_{Al}^{revis} (TPa)	ρ_{Al}^{revis}/ρ_0
11.69 ± 0.45[86]	5.009	13.87 ± 0.44[86]	6.606	6.600[95] ± 0.329[a]	6.703 ± 0.560	0.252 ± 0.029	1.935 ± 0.208
12.90 ± 0.46[86]	5.910	15.59 ± 0.38[86]	8.096	7.650[95] ± 0.330[a]	7.828 ± 0.566	0.331 ± 0.032	2.008 ± 0.196
15.02 ± 0.54[86]	7.490	17.81 ± 0.49[86]	10.02	9.780[95] ± 0.443[a]	9.903 ± 0.680	0.478 ± 0.046	2.252 ± 0.271
16.17 ± 0.48[86]	8.347	19.17 ± 0.51[86]	11.20	11.02[95] ± 0.44[a]	11.01 ± 0.62	0.572 ± 0.047	2.348 ± 0.263
17.08 ± 0.40[86]	9.027	19.75 ± 0.40[86]	11.70	12.14[95] ± 0.38[a]	11.96 ± 0.52	0.640 ± 0.041	2.534 ± 0.248
22.69 ± 0.49[86]	13.30	26.45 ± 0.44[86]	17.46	17.70[95] ± 0.48[a]	17.42 ± 0.66	1.250 ± 0.068	2.930 ± 0.308
17.35 ± 0.30[89]	9.229	20.90 ± 0.40[89]	12.70	12.20[89] ± 0.31[a]	12.09 ± 0.40	0.685 ± 0.036	2.371 ± 0.170
20.19 ± 0.25[90]	11.37	24.17 ± 0.40[90]	15.52	15.08[90] ± 0.31[a]	14.85 ± 0.35	0.973 ± 0.039	2.592 ± 0.166
36.77 ± 0.50[87]	24.86	43.57 ± 0.60[87]	32.05	30.72[87] ± 0.59[a]	31.94 ± 0.74	3.774 ± 0.139	3.746 ± 0.379
41.79 ± 0.60[87]	29.13	49.45 ± 0.70[87]	37.13	36.16[87] ± 0.73[a]	37.23 ± 0.88	4.993 ± 0.189	4.047 ± 0.466
42.63 ± 0.70[87]	29.84	50.58 ± 0.70[87]	38.10	36.89[87] ± 0.79[a]	38.09 ± 1.01	5.225 ± 0.210	4.050 ± 0.497
54.90 ± 0.60[87]	40.20	65.22 ± 0.60[87]	50.53	49.36[87] ± 0.71[a]	50.85 ± 0.85	8.994 ± 0.234	4.538 ± 0.417
62.65 ± 0.60[87]	46.65	75.03 ± 0.70[87]	58.72	56.96[87] ± 0.76[a]	58.70 ± 0.86	11.94 ± 0.29	4.595 ± 0.397
66.74 ± 0.60[87]	50.03	80.11 ± 0.80[87]	62.93	60.99[87] ± 0.82[a]	62.83 ± 0.88	13.65 ± 0.33	4.636 ± 0.404
71.25 ± 0.60[87]	53.73	85.98 ± 0.80[87]	67.77	65.40[87] ± 0.82[a]	67.32 ± 0.87	15.70 ± 0.35	4.607 ± 0.370
88.20 ± 0.70[87]	67.45	107.1 ± 0.9[87]	84.98	81.91[87] ± 0.95[a]	84.19 ± 1.00	24.45 ± 0.50	4.674 ± 0.348
120.0 ± 2.0[88]	92.82	147.0 ± 2.0[88]	116.8	116.7[88] ± 2.5[a]	115.6 ± 2.8	46.06 ± 1.73	4.682 ± 0.650
286.0 ± 4.0[88]	230.0	353.0 ± 4.0[88]	279.7	283.2[88] ± 5.1[a]	284.6 ± 5.3	272.2 ± 8.1	5.154 ± 0.641
291.0 ± 5.0[88]	234.0	366.0 ± 6.0[88]	290.3	288.3[88] ± 6.8[a]	288.1 ± 6.7	285.7 ± 11.3	4.693 ± 0.687
298.0 ± 4.0[88]	239.5	379.0 ± 5.0[88]	300.8	293.6[88] ± 5.5[a]	294.0 ± 5.2	302.1 ± 9.5	4.461 ± 0.484
344.0 ± 6.0[88]	276.4	441.0 ± 6.0[88]	350.1	338.9[88] ± 7.5[a]	338.5 ± 8.2	404.6 ± 15.2	4.300 ± 0.534

[a]Error is estimated as $\Delta U/U = \sqrt{(\Delta D_{Fe}/D_{Fe})^2 + (\Delta D_{Al}/D_{Al})^2}$.

mean free path. Typically, a gold *hohlraum* wall is used in an experiment. Some attempts to choose more effective compositions have been made, where authors proposed a composition of gold and gadolinium, Au 50%–Gd 50% (hereinafter, all percents in proportions of mixtures are by weight), as an alternative to pure gold.[96] Later, more complicated compositions were proposed.[97] However, this is not a complete solution of the problem. A more productive approach is the creation of mathematical methods and computer code to optimize the radiation yield from complex materials. This work has been performed by using the ion model of plasma.[98]

Before using the constructed optimization method for gold plasma, test calculations were made for the simpler case of copper plasma. The calculations for copper plasma were carried out at temperature $T = 50$ eV and density $\rho = 0.01$ g/cm^3. The optimal chemical composition A (Cu 22.9%–Co 28.9%–Mn 24%–V 14.1%–Sc 10.1%) was found. The Rosseland mean free path for copper plasma $L_R^{Cu} = 218\,\mu$m and for optimal composition $L_R^{oA} = 63.4\,\mu$m, and the ratio $L_R^{Cu}/L_R^{oA} = 3.44$.

Figure 6 presents the spectral coefficient for x-ray absorption K as a function of $\hbar\omega/T$ ($\hbar$ is the reduced Planck constant, ω is the angular frequency of the photon) calculated for Cu and for the composition A at temperature $T = 50$ eV and density $\rho = 0.01$ g/cm^3. One can see that spectral lines of composition A overlap this energy interval. This leads to a decrease in the Rosseland mean free path.

Further, the calculations were made for gold plasma[98] at $T = 250$ eV and $\rho = 1$ g/cm^3. The optimal chemical composition B (Au 25.7%–W 23.1%–Gd 18.1%–Pr 10.0%–Ba 10.4%–Sb 12.7%) was found. The Rosseland mean free path for gold plasma $L_R^{Au} = 5.01\,\mu$m and for optimal composition $L_R^{oB} = 1.61\,\mu$m, the ratio $L_R^{Au}/L_R^{oB} = 3.11$, whereas the composition of gold and gadolinium provides only ratio 1.74.[98]

As is known,[96] high power laser pulse interaction with a *hohlraum* wall produces optically thick plasmas, and the optimization problem was solved for this case. However, this problem can be solved as well for optically thin plasma arising from X-pinch.[99]

B. Estimation of radiative efficiency of complex materials for optically thin plasma in X-pinch

It is known that exploding wires in X-pinch produce optically thin plasma.[99] In this case, the outward energy flux of soft x-ray

TABLE IV. Same as in Table III but for experiments[84,85] with Mo–Al pairs.

D_{Mo} (km/s)	U_{Mo}^{theor} (km/s)	D_{Al} (km/s)	U_{Al}^{theor} (km/s)	$U_{Al}^{of\ ref}$ (km/s)	U_{Al}^{revis} (km/s)	P_{Al}^{revis} (TPa)	ρ_{Al}^{revis}/ρ_0
27.16 ± 0.41[84]	18.24	34.39 ± 0.69[84]	24.12	23.89 ± 0.65[84]	24.57 ± 0.63	2.289 ± 0.105	3.497 ± 0.401
30.60 ± 0.43[85]	21.10	39.41 ± 0.63[85]	28.44	27.57 ± 0.60[85]	28.18 ± 0.65	2.998 ± 0.117	3.494 ± 0.341

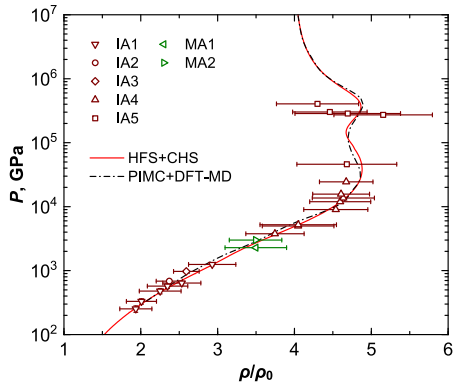

FIG. 5. The principal Hugoniot curve of Al in P–ρ/ρ_0 plane in comparison with revised data of relative measurements[84–90] from Tables III and IV and the PIMC+DFT-MD calculation results.[82] Equations of state of Al and standard materials (Fe, Mo) are calculated using the HFS electronic model with the CHS ionic part. Data are denoted similarly to Fig. 2.

radiation increases inversely proportionally to the Planck mean free path l_P:[38]

$$j \propto l_P^{-1}. \tag{9}$$

Therefore, the optimal chemical composition can be found by minimizing the Planck mean free path. We used this formula to estimate the relative radiation efficiency of two exploding wires made of materials A and B, respectively.

To test the ion model of plasma, calculations of radiative properties were performed for a NiCr alloy (Ni 80%–Cr 20%) and the so-called Alloy 188 (Cr 21.72%–Ni 22.92%–Fe 2.24%–Co 39%–W 13.93%). Later, the relative radiation efficiency of these materials was measured in an experiment at the Cornell University, Ithaca, New York.[100]

The total energy yield was measured using two devices with different energy bands, and the relative energy yield was compared with theoretical calculations. The deviations of the theoretical results from experimental data were from 3.2% to 5.6% depending on the specific experimental devices.

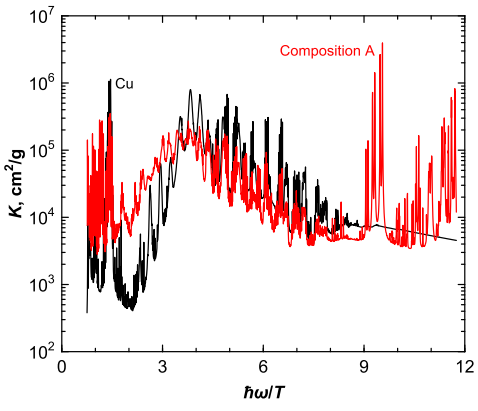

FIG. 6. The spectral coefficient for x-ray absorption K as a function of $\hbar\omega/T$ calculated for Cu (black line) and for the composition A (red line) at $T = 50$ eV and $\rho = 0.01$ g/cm^3.

C. Modeling of radiative and gas-dynamic processes in plasma for experiments, where both intense laser and heavy ion beams are used: Au-doping effect

The quantum-statistical approach has been successfully applied to theoretical and experimental studies of radiative and gas-dynamic processes in plasma, where both intense laser and heavy ion beams are used.[101]

As is known, the intensity of heavy ion beam interaction with a target increases, if the target is heated up to a plasma state.[28–30] In such experiments, the plasma target should keep a fixed temperature and density during further interaction with heavy ion beam, which is produced by an accelerator. For the plasma generation, so-called indirect heating of CHO polymer foam with laser pulse is used. At first, the laser pulse interacts with the Au cylindrical converter-*hohlraum*, and then the x-ray radiation produced heats the porous CHO polymer slab.

A separate numerical simulation was performed under specific experimental conditions. It showed that the CHO plasma target, which is made of cellulose triacetate $C_{12}H_{16}O_8$ (TAC), really keeps its temperature at 20 eV and density at 0.003 g/cm^3 for 6 ns. That is enough to enable its interaction with the heavy ion beam.

A numerical simulation was also performed for the experiment where *hohlraum* radiation transmits through the TAC target for 5 ns. It was found that 75% of the radiation energy was absorbed in the target, and this value agrees well with the measured value.[101] In reality, it is possible to increase the portion of absorbed energy to boost the intensity of the heavy ion beam interaction with the target. The so-called Au-doping effect can be used to this end.[45]

A small admixture of gold can be added to the TAC plasma, and this admixture can considerably influence the amount of absorbed energy. The Rosseland mean free path l_R was calculated as a function of the plasma temperature T for TAC plasma and for two different plasma compositions, namely TAC 99.3%–Au 0.7% and TAC 98.6%–Au 1.4%. Figure 7 presents the calculations, which were performed at the plasma densities 0.005 and 0.001 g/cm^3.

The explanation of this effect is connected to the behavior of the Rosseland mean free path during the process of plasma heating by x-ray radiation. At the initial stage of heating, the plasma temperature in the target is small and the Rosseland mean free path is small as well. Therefore, practically all radiation is absorbed in the target. During the next stage, the temperature increases and the Rosseland mean free path increases too, and some photons can go through the target taking away the energy. Nevertheless, one can suppress this process adding a little admixture of gold to the TAC plasma. As has been found, this can lead to approximately a halving of the value of the Rosseland mean free path. This effect is demonstrated for different plasma densities and different admixture of gold concentrations in Fig. 7.

D. Modern method of temperature diagnostics for X- and Z-pinch plasmas

Temperature diagnosis of plasma is necessary in numerous investigations of matter in a high energy density state. Some methods of generation of plasma with high energy density parameters are described in Refs. 102 and 103.

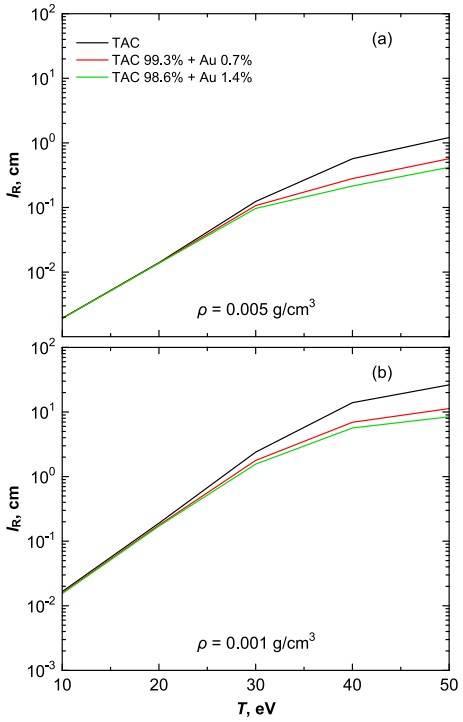

FIG. 7. The calculated Rosseland mean free path l_R as a function of the plasma temperature T for TAC (black line) and for two different plasma compositions, namely TAC 99.3%–Au 0.7% (red line) and TAC 98.6%–Au 1.4% (green line) at the plasma densities (a) 0.005 and (b) 0.001 g/cm^3.

A rather complicated problem is connected with temperature diagnosis of plasma that is produced in X- and Z-pinches.[103] Traditional methods for diagnosing the plasma temperature are based on the analysis of the shape of spectral lines. In this case, the intervals of radiation energies are used where the spectral lines are well differentiated in the experiment.[104] Comparison of measured spectral line shape, intensity, and width with those calculated at different temperatures and densities makes it possible to diagnose these plasma parameters.

Unfortunately, traditional methods of temperature diagnosis encounter problems in practice. If the plasma temperature increases up to 3 or 4 keV, the spectral lines become practically indistinguishable. Calculations of the intensity and width of spectral lines for substances with a large nuclear charge Z is a difficult problem as well.

However, a modern method for the diagnosis has been proposed.[105] The spectral brightness of radiation can be calculated across a large interval of photon energies. In this case, one can find out the photon energy range where this function has high sensitivity to the temperature variation. The ion model of plasma provides reliable quantum-statistical calculations of plasma properties over a wide range of temperatures and densities. In particular, the spectral brightness of x-ray radiation can be calculated across a large interval of photon energy over a wide range of plasma parameters.

Let us consider the mechanism of Z-pinch explosion of wires or foils. This process typically yields several bright, x-ray emitting micropinches at random locations along the conductor.[106] This phenomenon is connected with the production of tiny drops of plasma, so-called hot spots, with high temperature and density.[106] During the first stage of plasma burning, the intensity of the x-ray radiation is relatively low because of the high density of plasma. During the next stage, the plasma drop extends and the plasma temperature simultaneously increases according to the energy of the electromagnetic field. The temperature diagnosis should be performed during this stage of plasma burning.

In the present work, we calculated the spectral brightness of the radiation of a titanium plasma at temperatures $T = 1$ and 1.2 keV, and at density $\rho = 0.906$ g/cm^3. This density value corresponds to a five times expansion of the initial plasma drop ($\rho_0/\rho = 5$, $\rho_0 = 4.53$ g/cm^3).

The spectral brightness of radiation $j_\nu(E)$ can be obtained in the framework of the approximation of a radiating ball with radius R_b as follows:

$$j_\nu(E) = \frac{1}{4\pi} cK(E)\rho U_\nu \frac{R_b}{3}, \tag{10}$$

where $K(E)$ is the spectral absorption coefficient for photons with energy $E = h\nu$ and frequency ν; ρ is the density of the plasma; c is the speed of light; and h is the Planck constant. The spectral density of equilibrium radiation U_ν is given by the formula[38]

$$U_\nu = \frac{8\pi h\nu^3}{c^3}\left[\exp\left(\frac{h\nu}{T}\right) - 1\right]^{-1}. \tag{11}$$

This approximation is correct for optically thin plasma only.

It should be noted that the characteristic size of radiating plasma could be experimentally measured. In particular, experimental results[107] give a characteristic size (diameter) of the source from 0.7 to 2.8 μm. In our calculations, the radius of the radiating ball was set as $R_b = 1$ μm.

The Planck mean free path was therefore calculated for the plasma density $\rho = 0.906$ g/cm^3 and the temperatures $T = 1$ and 1.2 keV. The Planck mean free path was found as $l_P = 64.8$ and 218 μm, respectively. In both cases, the Planck mean free path exceeds the geometrical size R_b of the radiating ball. This means that the approximation of optically thin plasma is correct for both cases.

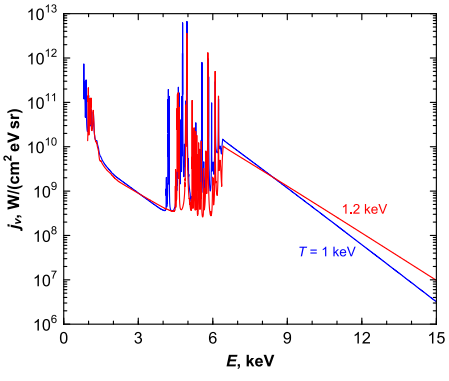

FIG. 8. The spectral brightness $j_\nu(E)$ of Ti plasma radiation calculated at the plasma density $\rho = 0.906$ g/cm^3 and the temperatures $T = 1$ (blue line) and 1.2 keV (red line).

Figure 8 shows the calculated spectral brightness $j_\nu(E)$ of Ti plasma radiation. One can see that the value of radiation spectral density j_ν for an energy value E of about 12 keV, which was calculated at $T = 1$ keV, is approximately twice the corresponding value calculated at $T = 1.2$ keV, although the difference in temperature is only 20%. In such a way, these calculations provide information about the interval of photon energies within which the spectral brightness has high sensitivity to temperature changes.

V. CONCLUSION

Amongst the quantum-statistical models considered in the framework of the approximation of the average atom, the HFS model has the widest range of agreement of calculation results with experimental data on thermodynamic properties of hot dense plasma. In particular, detailed analysis of data from the relative measurements of the compressibility of different substances by means of the HFS model provides the observation that shell effects have a significant influence on the thermodynamic properties of the plasma.

In contrast to previous theoretical models that use the approximation of average-atom and different additional physical approximations to simplify the mathematical calculations, the general set of self-consistent field equations, which describe the quantum states of the entire ensemble of plasma atoms and ions, is solved in the framework of the ion model of plasma. It provides reliable quantum-statistical calculations of the radiative properties over a wide range of densities and temperatures. Some successful applications of this modern quantum-statistical model have been presented above.

ACKNOWLEDGMENTS

The work is supported by the Presidium RAS within the framework of the basic research program No. 6 "New approaches to the creation and study of extreme states of matter."

REFERENCES

[1]S. Yu. Gus'kov, "Thermonuclear gain and parameters of fast ignition ICF-targets," Laser Part. Beams **23**, 255–260 (2005).
[2]A. Bret and C. Deutsch, "Density gradient effects on beam plasma linear instabilities for fast ignition scenario," Laser Part. Beams **24**, 269–273 (2006).
[3]H. Sakagami, T. Johzaki, H. Nagamoto, and K. Mima, "Fast ignition integrated interconnecting code project for cone-guided targets," Laser Part. Beams **24**, 191–198 (2006).
[4]D. Batani, R. Dezulian, R. Redaelli, R. Benocci, H. Stabile *et al.*, "Recent experiments on the hydrodynamics of laser-produced plasmas conducted at the PALS laboratory," Laser Part. Beams **25**, 127–141 (2007).
[5]G. V. Sin'ko, N. A. Smirnov, A. A. Ovechkin, P. R. Levashov, and K. V. Khishchenko, "Thermodynamic functions of the heated electron subsystem in the field of cold nuclei," High Energy Density Phys. **9**, 309–314 (2013).
[6]A. A. Ovechkin, P. A. Loboda, V. G. Novikov, A. S. Grushin, and A. D. Solomyannaya, "RESEOS—a model of thermodynamic and optical properties of hot and warm dense matter," High Energy Density Phys. **13**, 20–33 (2014).
[7]A. A. Charakhch'yan and K. V. Khishchenko, "Plane thermonuclear detonation waves initiated by proton beams and quasi-one-dimensional model of fast ignition," Laser Part. Beams **33**, 65–80 (2015).
[8]N. E. Andreev, M. E. Povarnitsyn, M. E. Veysman, A. Ya. Faenov, P. R. Levashov *et al.*, "Interaction of annular-focused laser beams with solid targets," Laser Part. Beams **33**, 541–550 (2015).
[9]K. V. Khishchenko, "Equation of state for tungsten over a wide range of densities and internal energies," J. Phys.: Conf. Ser. **653**, 012081 (2015).
[10]C. A. McCoy, M. D. Knudson, and S. Root, "Absolute measurement of the Hugoniot and sound velocity of liquid copper at multimegabar pressures," Phys. Rev. B **96**, 174109 (2017).
[11]S. Zhang, B. Militzer, L. X. Benedict, F. Soubiran, P. A. Sterne, and K. P. Driver, "Path integral Monte Carlo simulations of dense carbon-hydrogen plasmas," J. Chem. Phys. **148**, 102318 (2018).
[12]L. V. Al'tshuler, R. F. Trunin, K. K. Krupnikov, and N. V. Panov, "Explosive laboratory devices for shock wave compression studies," Usp. Fiz. Nauk **166**, 575–581 (1996).
[13]A. I. Funtikov, "Explosive laboratory measurement of the dynamical compressibility of porous substances in the pressure range from 0.1 to 1 TPa," Usp. Fiz. Nauk **167**, 1119–1120 (1997).
[14]D. Nikolaev, V. Ternovoi, V. Kim, and A. Shutov, "Plane shock compression generators, utilizing convergence of conical shock waves," J. Phys.: Conf. Ser. **500**, 142026 (2014).
[15]M. D. Knudson, R. W. Lemke, D. B. Hayes, C. A. Hall, C. Deeney, and J. R. Asay, "Near-absolute Hugoniot measurements in aluminum to 500 GPa using a magnetically accelerated flyer plate technique," J. Appl. Phys. **94**, 4420–4431 (2003).
[16]V. V. Alexandrov, A. V. Branitskii, E. V. Grabovski, Ya. N. Laukhin, G. M. Oleinik *et al.*, "Acceleration of metallic flyers at Angara-5-1 facility," Phys. At. Nucl. **81**, 1586–1589 (2018).
[17]S. Yu. Gus'kov, "Fast ignition of inertial confinement fusion targets," Plasma Phys. Rep. **39**, 1–50 (2013).
[18]K. V. Khishchenko and A. A. Charakhch'yan, "On some features of plane waves of thermonuclear burn," J. Appl. Mech. Tech. Phys. **56**, 86–95 (2015).
[19]K. Lan, J. Liu, Z. Li, X. Xie, W. Huo *et al.*, "Progress in octahedral spherical hohlraum study," Matter Radiat. Extremes **1**, 8–27 (2016).
[20]R. Betti and O. A. Hurricane, "Inertial-confinement fusion with lasers," Nat. Phys. **12**, 435–448 (2016).
[21]I. K. Krasyuk, P. P. Pashinin, A. Yu. Semenov, K. V. Khishchenko, and V. E. Fortov, "Study of extreme states of matter at high energy densities and high strain rates with powerful lasers," Laser Phys. **26**, 094001 (2016).
[22]T. A. Shelkovenko, S. A. Pikuz, I. N. Tilikin, M. D. Mitchell, S. N. Bland, and D. A. Hammer, "Evolution of X-pinch loads for pulsed power generators with current from 50 to 5000 kA," Matter Radiat. Extremes **3**, 267–277 (2018).
[23]R. B. Baksht, V. I. Oreshkin, A. G. Rousskikh, and A. S. Zhigalin, "Energy balance in a Z pinch with suppressed Rayleigh–Taylor instability," Plasma Phys. Controlled Fusion **60**, 035015 (2018).
[24]X. Wang, "Research at Tsinghua University on electrical explosions of wires," Matter Radiat. Extremes **4**, 017201 (2019).
[25]V. V. Ivanov, A. A. Anderson, and D. Papp, "Investigation of wire-array Z-pinches by laser probing diagnostics," Matter Radiat. Extremes **4**, 017401 (2019).
[26]V. M. Romanova, A. R. Mingaleev, A. E. Ter-Oganesyan, T. A. Shelkovenko, G. V. Ivanenkov, and S. A. Pikuz, "Core structure and secondary breakdown of an exploding wire in the current-pause regime," Matter Radiat. Extremes **4**, 026401 (2019).
[27]D. Yanuka, S. Theocharous, S. Efimov, S. N. Bland, A. Rososhek *et al.*, "Synchrotron based x-ray radiography of convergent shock waves driven by underwater electrical explosion of a cylindrical wire array," J. Appl. Phys. **125**, 093301 (2019).
[28]D. H. H. Hoffmann, A. Blazevic, P. Ni, O. Rosmej, M. Roth *et al.*, "Present and future perspectives for high energy density physics with intense heavy ion and laser beams," Laser Part. Beams **23**, 47–53 (2005).
[29]A. M. Khalenkov, N. G. Borisenko, V. N. Kondrashov, Yu. A. Merkuliev, J. Limpouch, and V. G. Pimenov, "Experience of micro-heterogeneous target fabrication to study energy transport in plasma near critical density," Laser Part. Beams **24**, 283–290 (2006).
[30]O. N. Rosmej, N. Zhidkov, V. Vatulin, N. Sulov, A. Kunin *et al.*, Experiments on heating of low Z targets by means of hohlraum radiation, in *GSI Scientific Report 2009*, edited by K. Grosse (GSI, Darmstadt, 2010), p. 387.
[31]S. F. Gnyusov, V. P. Rotshtein, A. E. Mayer, V. V. Rostov, A. V. Gunin *et al.*, "Simulation and experimental investigation of the spall fracture of 304L stainless steel irradiated by a nanosecond relativistic high-current electron beam," Int. J. Fract. **199**, 59–70 (2016).

[32]S. A. Barengolts, V. G. Mesyats, V. I. Oreshkin, E. V. Oreshkin, K. V. Khishchenko *et al.*, "Mechanism of vacuum breakdown in radio-frequency accelerating structures," Phys. Rev. Accel. Beams **21**, 061004 (2018).
[33]L. V. Al'tshuler, B. N. Moiseev, L. V. Popov, G. V. Simakov, and R. F. Trunin, "Relative compressibility of iron and lead at pressures of 31 to 34 Mbar," Sov. Pys. JETP **27**, 420–422 (1968).
[34]C. E. Ragan, M. G. Silbert, and B. C. Diven, "Shock compression of molybdenum to 2.0 TPa by means of a nuclear explosion," J. Appl. Phys. **48**, 2860–2870 (1977).
[35]A. C. Mitchell, W. J. Nellis, R. A. Heinle, G. W. Repp, J. A. Moriarty *et al.*, "Shock-impedance-match experiments at pressures to 2.5 TPa (25 Mbar)," Physica B+C **139**, 591–594 (1986).
[36]E. N. Avrorin, B. K. Vodolaga, V. A. Simonenko, and V. E. Fortov, "High-intensity shock-waves and the extreme states of matter," Usp. Fiz. Nauk **163**, 1–34 (1993).
[37]R. F. Trunin, "Shock compression of condensed matters in strong shock-waves caused by underground nuclear-explosions," Usp. Fiz. Nauk **164**, 1215–1237 (1994).
[38]Ya. B. Zel'dovich and Yu. P. Raizer, *Physics of Shock Waves and High-Temperature Hydrodynamic Phenomena* (Academic Press, New York, 1967).
[39]P. Adamek, O. Renner, L. Drska, F. B. Rosmej, and J. F. Wyart, "Genetic algorithms in spectroscopic diagnostics of hot dense plasmas," Laser Part. Beams **24**, 511–518 (2006).
[40]I. V. Lomonosov, "Multi-phase equation of state for aluminum," Laser Part. Beams **25**, 567–584 (2007).
[41]M. E. Povarnitsyn, N. E. Andreev, P. R. Levashov, K. V. Khishchenko, D. A. Kim *et al.*, "Laser irradiation of thin films: Effect of energy transformation," Laser Part. Beams **31**, 663–671 (2013).
[42]I. V. Lomonosov and S. V. Fortova, "Wide-range semiempirical equations of state of matter for numerical simulation on high-energy processes," High Temp. **55**, 585–610 (2017).
[43]A. F. Nikiforov, V. G. Novikov, and V. B. Uvarov, *Quantum-Statistical Models of Hot Dense Matter* (Birkhäuser, Basel, 2005).
[44]N. Yu. Orlov, "A method of calculating selfconsistent potentials for a mixture of chemical elements," USSR Comput. Math. Math. Phys. **26**, 165–170 (1986).
[45]N. Yu. Orlov, O. B. Denisov, G. A. Vergunova, and O. N. Rozmej, "Mathematical modeling of the Au-doping effect on the radiative properties of porous polymers in experiments with laser and heavy-ion beams," J. Russ. Laser Res. **35**, 119–123 (2014).
[46]N. H. March, W. H. Young, and S. Sampanthar, *The Many-Body Problem in Quantum Mechanics* (Cambridge University Press, Cambridge, 1967).
[47]W. Kohn and P. Vashishta, "General density functional theory," in *Theory of the Inhomogeneous Electron Gas, Physics of Solids and Liquids*, edited by S. Lundqvist and N. H. March (Springer, Boston, MA, 1983).
[48]A. K. Radjagopal, "Theory of inhomogeneous electron systems: Spin-density-functional formalism," Adv. Chem. Phys. **41**, 59–193 (1980).
[49]N. Yu. Orlov and V. E. Fortov, "Comparative analysis of the theoretical models of a hot dense plasma and the density functional theory," Plasma Phys. Rep. **27**, 44–55 (2001).
[50]N. Yu. Orlov, "Quantum-statistical calculation of the properties of a mixture of chemical elements allowing for fluctuations in the occupation numbers of electron states," USSR Comput. Math. Math. Phys. **27**, 64–70 (1987).
[51]N. Yu. Orlov, "Ion model of a hot dense plasma," Laser Part. Beams **15**, 627–634 (1997).
[52]L. H. Thomas, "The calculation of atomic fields," Math. Proc. Cambridge Philos. Soc. **23**, 542–548 (1927).
[53]E. Fermi, "Statistical method to determine some properties of atoms," Rend. Accad. Naz. Lincei **6**, 602–607 (1927).
[54]R. P. Feynman, N. Metropolis, and E. Teller, "Equations of state of elements based on the generalized Fermi–Thomas theory," Phys. Rev. **75**, 1561–1573 (1949).
[55]D. A. Kirzhnits, "Quantum corrections to the Thomas–Fermi equation," Sov. Phys. JETP **5**, 64–71 (1957).
[56]N. N. Kalitkin, "The Thomas–Fermi model of the atom with quantum and exchange corrections," Sov. Phys. JETP **11**, 1106–1110 (1960).
[57]B. F. Rozsnyai, "Relativistic Hartree–Fock–Slater calculations for arbitrary temperature and matter density," Phys. Rev. A **5**, 1137–1149 (1972).
[58]A. F. Nikiforov and V. B. Uvarov, "Description of the state of matter at high temperatures based on equations of the self-consistent field," Chislennye Metody Mekh. Sploshnoi Sredy **4**, 114–117 (1973).
[59]B. F. Rozsnyai, "An overview of the problems connected with theoretical calculations for hot plasmas," J. Quant. Spectrosc. Radiat. Transfer **27**, 211–217 (1982).
[60]J. Zeng, F. Jin, and J. Yuan, "Radiative opacity of plasmas studied by detailed term (level) accounting approaches," Front. Phys. China **1**, 468–489 (2006).
[61]A. V. Bushman and V. E. Fortov, "Models of equation of the matter state," Usp. Fiz. Nauk **140**, 177–232 (1983).
[62]F. Perrot, "Hartree–Fock study of the ground-state energy and band structure of metallic copper," Phys. Rev. B **11**, 4872–4884 (1975).
[63]M. A. Kadatskiy and K. V. Khishchenko, "Theoretical investigation of the shock compressibility of copper in the average-atom approximation," Phys. Plasmas **25**, 112701 (2018).
[64]S. I. Anisimov, A. M. Prokhorov, and V. E. Fortov, "The use of powerful lasers for the study of matter under superhigh pressures," Usp. Fiz. Nauk **142**, 395–434 (1984).
[65]V. A. Alekseyev, V. E. Fortov, and I. T. Yakubov, "Physical properties of high-pressure plasma," Usp. Fiz. Nauk **139**, 193–222 (1983).
[66]W. Ebeling, "Nonideality effects in plasmas with multiply charged ions," Contrib. Plasma Phys. **29**, 165–172 (1989).
[67]V. G. Novikov, "Inclusion of individual states of ions in the modified Hartree–Fock–Slater model," High Temp. **30**, 573–578 (1992).
[68]L. D. Landau and E. M. Lifshitz, *Statistical Physics. Part 1* (Pergamon, Oxford, 1980).
[69]J. P. Hansen, "Statistical mechanics of dense ionized matter. I. Equilibrium properties of the classical one-component plasma," Phys. Rev. A **8**, 3096–3109 (1973).
[70]R. G. Palmer and J. D. Weeks, "Exact solution of the mean spherical model for charged hard spheres in a uniform neutralizing background," J. Chem. Phys. **58**, 4171–4174 (1973).
[71]N. N. Kalitkin, L. V. Kuzmina, and A. I. Funtikov, "The main Hugoniot-curves of 10 metals," Mat. Model. **14**, 27–42 (2002).
[72]L. V. Al'tshuler, S. B. Kormer, A. A. Bakanova, and R. F. Trunin, "Equation of state for aluminum, copper, and lead in the high pressure region," Sov. Phys. JETP **11**, 573–579 (1960).
[73]R. H. Warnes, "Shock wave compression of three polynuclear aromatic compounds," J. Chem. Phys. **53**, 1088–1094 (1970).
[74]L. V. Al'tshuler, A. A. Bakanova, I. P. Dudoladov, E. A. Dynin, R. F. Trunin, and B. S. Chekin, "Shock adiabatic curves of metals," J. Appl. Mech. Tech. Phys. **22**, 145–169 (1981).
[75]A. C. Mitchell and W. J. Nellis, "Shock compression of aluminum, copper, and tantalum," J. Appl. Phys. **52**, 3363–3374 (1981).
[76]R. F. Trunin, L. F. Gudarenko, M. V. Zhernokletov, and G. V. Simakov, *Experimental Data on Shock-Wave Compression and Adiabatic Expansion of Condensed Substances*, 2nd ed. (RFNC-VNIITF, Sarov, 2006), pp. 24–25.
[77]M. A. Kadatskiy and K. V. Khishchenko, "Comparison of Hugoniots calculated for aluminum in the framework of three quantum-statistical models," J. Phys.: Conf. Ser. **653**, 012079 (2015).
[78]V. A. Simonenko, N. P. Voloshin, A. S. Vladimirov, A. P. Nagibin, V. N. Nogin *et al.*, "Absolute measurements of shock compressibility of aluminum at pressures $P \gtrsim 1$ TPa," Zh. Eksp. Teor. Fiz. **88**, 1452–1459 (1985).
[79]L. P. Volkov, N. P. Voloshin, A. S. Vladimirov, V. N. Nogin, and V. A. Simonenko, "Shock compressibility of aluminum at a pressure of 10 Mbar," JETP Lett. **31**, 588–592 (1980).
[80]M. A. Podurets, V. M. Ktitorov, R. F. Trunin, L. V. Popov, A. Ya. Matveev *et al.*, "Shock-wave compression of aluminum at pressures of 1.7 TPa," High Temp. **32**, 890–892 (1994).
[81]V. A. Simonenko, "Experimental measurements of equation of state for metals to 200 Mbar and comparison with Thomas–Fermi and other theoretical models," High Pressure Sci. Technol. **5**, 816–818 (1990).

[82]K. P. Driver, F. Soubiran, and B. Militzer, "Path integral Monte Carlo simulations of warm dense aluminum," Phys. Rev. E **97**, 063207 (2018).
[83]R. F. Trunin, G. V. Simakov, M. A. Podurets, B. N. Moiseyev, and L. V. Popov, "Dynamic compressibility of quartz and quartzite at high pressure," Izv. Acad. Sci. USSR Phys. Solid Earth **1**, 8–11 (1971).
[84]C. E. Ragan, "Shock compression measurements at 1 to 7 TPa," Phys. Rev. A **25**, 3360–3375 (1982).
[85]C. E. Ragan, "Shock-wave experiments at threefold compression," Phys. Rev. A **29**, 1391–1402 (1984).
[86]E. N. Avrorin, B. K. Vodolaga, N. P. Voloshin, G. V. Kovalenko, V. F. Kuropatenko *et al.*, "Experimental study of shell effects for shock adiabates of condensed substances," Zh. Eksp. Teor. Fiz. **93**, 613–626 (1987).
[87]E. N. Avrorin, B. K. Vodolaga, N. P. Voloshin, V. F. Kuropatenko, G. V. Kovalenko *et al.*, "Experimental confirmation of shell effects on the shock adiabats of aluminum and lead," JETP Lett. **43**, 308–311 (1986).
[88]A. S. Vladimirov, N. P. Voloshin, V. N. Nogin, A. V. Petrovtsev, and V. A. Simonenko, "Shock compressibility of aluminum at $p \gtrsim 1$ Gbar," JETP Lett. **39**, 82–85 (1984).
[89]R. F. Trunin, N. V. Panov, and A. B. Medvedev, "Shock compressibility of iron, aluminum, and tantalum under terapascal pressures in laboratory conditions," High Temp. **33**, 328–329 (1995).
[90]R. F. Trunin, N. V. Panov, and A. B. Medvedev, "Compressibility of iron, aluminum, molybdenum, titanium, and tantalum at shock-wave pressures of 1–2.5 TPa," JETP Lett. **62**, 591–594 (1995).
[91]M. A. Kadatskiy and K. V. Khishchenko, "Shock compressibility of iron calculated in the framework of quantum-statistical models with different ionic parts," J. Phys.: Conf. Ser. **774**, 012005 (2016).
[92]M. A. Kadatskiy and K. V. Khishchenko, Shock compressibility of SiO_2 calculated in the framework of quantum-statistical models, in *Scientific Coordination Workshop on Non-Ideal Plasma Physics, November 27-28, 2015, Moscow, Russia, Book of Abstracts*, edited by V. E. Fortov (JIHT RAS, Moscow, 2015), pp. 15–16.
[93]M. V. Zhernokletov, A. B. Medvedev, and G. V. Simakov, "Isentropes of unloading and the equation of molybdenum state at high-energy densities," Khim. Fiz. **14**(2–3), 49–55 (1995).
[94]L. V. Al'tshuler, "Use of shock waves in high-pressure physics," Sov. Phys. Usp. **8**, 52–91 (1965).
[95]R. F. Trunin, M. A. Podurets, G. V. Simakov, L. V. Popov, and A. G. Sevast'yanov, "New data on aluminum, plexiglas and quartz compressibility obtained during strong shock-waves of underground nuclear-explosion," Zh. Eksp. Teor. Fiz. **108**, 851–861 (1995).
[96]T. J. Orzechowski, M. D. Rosen, H. N. Kornblum, J. L. Porter, L. J. Suter *et al.*, "The Rosseland mean opacity of a mixture of gold and gadolinium at high temperatures," Phys. Rev. Lett. **77**, 3545–3548 (1996).
[97]D. A. Callahan-Miller and M. Tabak, "Progress in target physics and design for heavy ion fusion," Phys. Plasmas **7**, 2083–2091 (2000).
[98]O. B. Denisov, N. Yu. Orlov, S. Yu. Gus'kov, V. B. Rozanov, N. V. Zmitrenko, and A. P. Mikhailov, "Modeling of the composition of materials for soft X-ray sources used in research on inertial confinement fusion," Plasma Phys. Rep. **31**, 684–689 (2005).
[99]D. B. Sinars, S. A. Pikuz, T. A. Shelkovenko, K. M. Chandler, D. A. Hammer, and J. P. Apruzese, "Time-resolved spectroscopy of Al, Ti, and Mo X pinch radiation using an X-ray streak camera," J. Quant. Spectrosc. Radiat. Transfer **78**, 61–83 (2003).
[100]N. Yu. Orlov, S. Yu. Gus'kov, S. A. Pikuz, V. B. Rozanov, T. A. Shelkovenko *et al.*, "Theoretical and experimental studies of the radiative properties of hot dense matter for optimizing soft X-ray sources," Laser Part. Beams **25**, 415–423 (2007).
[101]N. Yu. Orlov, O. B. Denisov, O. N. Rosmej, D. Schäfer, Th. Nisius *et al.*, "Theoretical and experimental studies of material radiative properties and their applications to laser and heavy ion inertial fusion," Laser Part. Beams **29**, 69–80 (2011).
[102]S. A. Pikuz, T. A. Shelkovenko, and D. A. Hammer, "X-pinch. Part I," Plasma Phys. Rep. **41**, 291–342 (2015).
[103]S. A. Pikuz, T. A. Shelkovenko, and D. A. Hammer, "X-pinch. Part II," Plasma Phys. Rep. **41**, 445–491 (2015).
[104]S. B. Hansen, A. S. Shlyaptseva, S. A. Pikuz, T. A. Shelkovenko, D. B. Sinars *et al.*, "Analysis of L-shell line spectra with 50-ps time resolution from Mo X-pinch plasmas," Phys. Rev. E **70**, 026402 (2004).
[105]N. Yu. Orlov, O. B. Denisov, and G. A. Vergunova, "Temperature diagnostics of a Z-pinch plasma using calculations of the spectral brightness of X-ray radiation in a large interval of radiation energies," J. Russ. Laser Res. **37**, 91–96 (2016).
[106]N. R. Pereira and J. Davis, "X rays from Z-pinches on relativistic electron-beam generators," J. Appl. Phys. **64**, R1–R27 (1988).
[107]I. N. Tilikin, T. A. Shelkovenko, S. A. Pikuz, and D. A. Hammer, "Determination of the size of a radiation source by the method of calculation of diffraction patterns," Opt. Spectrosc. **115**, 128–136 (2013).
[108]M. A. Kadatskiy, "Quantum-statistical calculations of the thermodynamic properties of molybdenum at high energy densities," High Energy Density Phys. **33**, 100700 (2019).